Journal of Energy Storage 55 (2022) 105459

Contents lists available at ScienceDirect

Journal of Energy Storage

journal homepage: www.elsevier.com/locate/est

Research papers

Screening double salt sulfate hydrates for application in thermochemical heat storage

W. Kooijman, D.J. Kok, M.A.R. Blijlevens, H. Meekes, E. Vlieg *

Radboud University, Institute for Molecules and Materials, Heyendaalseweg 135, 6525 ED Nijmegen, the Netherlands

ARTICLE INFO

Keywords:
Thermochemical heat storage
Double sulfate salt hydrates
Domestic heat storage
Thermochemical analysis
Hydration/dehydration cyclability

ABSTRACT

In this paper a relatively new class of thermochemical compounds is tested for their heat storage potential. 24 different double salt sulfate hydrates with the general formula $A^{I}_{2}B^{II}(SO_4)_2{\cdot}nH_2O$ were synthesized and screened for the desirable properties of a thermochemical heat battery material. The materials were tested on the following set of criteria: energy density $\geq$ 1.3 GJ/m^3, dehydration temperature $\leq$ 120 °C, 10-fold cyclability at $P_{H2O} \leq$ 12 mbar. The 24 salts have dehydration temperatures between 55 and 198 °C and energy densities between 1.1 and 2.0 GJ/m^3. $(NH_4)_2Zn(SO_4)_2{\cdot}6H_2O$ is the only material that passes all the set criteria and is therefore suitable for further investigation. This material has an energy density of 1.78 GJ/m^3, a dehydration temperature of 84 °C after one dehydration-hydration cycle and can perform at least 10 cycles without loss of performance. There are five other salts of interest that meet two out of the three criteria. $(NH_4)_2Ni(SO_4)_2{\cdot}6H_2O$ has a 1.8 GJ/m^3 energy density and is cyclable 10 times, but has a dehydration temperature of 132 °C. $(NH_4)_2Fe(SO_4)_2{\cdot}6H_2O$, $(NH_4)_2Mg(SO_4)_2{\cdot}6H_2O$, $Cs_2Mg(SO_4)_2{\cdot}6H_2O$ and $Cs_2Ni(SO_4)_2{\cdot}6H_2O$ have energy densities of 1.6 to 1.76 GJ/m^3 and dehydration temperatures below 120 °C, but they require 22.7 mbar to achieve cyclability.

1. Introduction

In the ongoing effort to transition to renewable energy sources, the need for different energy storage methods has become apparent, since renewable energy sources like wind or solar energy are only intermittently available, and not on demand. The best-known example of such a storage technology is probably the electrical battery, but recently heat storage has become a focus of research as well, as about 80 % of the energy used in domestic houses is used for hot water and space heating [1]. With heat storage it is possible to utilize industrial waste heat, but it is also possible to store a surplus of renewable energy in the form of heat for domestic heating [2].

There are three main heat storage methods. In sensible heat storage (SHS), a storage material is heated up and kept in an insulated environment until the heat is needed. Thermal insulation, however, is never perfect and so this method has limited capacity for long term storage due to thermal leakage. In case of latent heat storage (LHS), the energy is stored in the heat of a phase transition, like the reversible solid to liquid transition of H_2O or paraffin. In the case of a thermochemical material (TCM), the heat is stored for an unlimited time in a reversible chemical reaction, most commonly the drying of a salt hydrate. In short, thermochemical heat storage works as follows: When excess heat is available, the hydrated salt is warmed up, releasing water in the form of vapor. When heat is required, water vapor is added to the dry salt and the hydrate is formed again in an exothermic reaction. By choosing appropriate salt hydrates this method offers a much higher energy density than SHS or LHS and has the additional advantages of long-term storage with little energy loss and a controllable release of the stored heat [3,4].

In a 2015 review on thermal energy storage Aydin et al. compared the state of the art of the three storage methods in terms of storage capacity, showing that the maximum capacity for SHS was <0.05 GJ/m^3 (for water), while for LHS applications the maximum capacity was limited to 0.1 GJ/m^3 (for paraffin wax). Thermochemical materials mentioned by Aydin et al. offered a larger storage capacity up to 0.18 GJ/m^3 for silica gel [5]. In later years studies on salt hydrates showed that the class of TCMs allows for even higher storage capacities. In 2017 Donkers et al. reported on a literature study compiling 563 TCM hydration/dehydration reactions of salt hydrates [4]. For a TCM to be suitable for use in a domestic setting, Donkers et al. published a list of thermodynamic criteria for TCM's intended for residential use, taking also into account the practical limitations for an actual thermo chemical

* Corresponding author.
E-mail address: e.vlieg@science.ru.nl (E. Vlieg).

https://doi.org/10.1016/j.est.2022.105459
Received 8 April 2022; Received in revised form 13 July 2022; Accepted 8 August 2022
Available online 23 August 2022
2352-152X/© 2022 The Authors. Published by Elsevier Ltd. This is an open access article under the CC BY license (http://creativecommons.org/licenses/by/4.0/).

Table 1
TCM screening criteria used here and based on Donkers et al. [4]

Criterion	Value
Energy density	≥1.3 GJ/m^3
Dehydration temperature	≤120 °C
Water vapor pressure during hydration	≤12 mbar
Number of cycles	≥10

storage device [4]. A well-insulated house has a typical yearly heat demand of 20 GJ. Due to the mismatch of heat demand and heat supply from the solar collectors there is a heat energy deficit of 10 GJ in the cold months [6]. The volume of the system was set to a maximum of 10 m^3 leading to a required system energy density of at least 1.0 GJ/m^3. The TCM itself should have an energy density of at least 1.3 GJ/m^3 to account for issues concerning valves, piping and tubing as well as the porosity of the material. To keep the charging process at a viable efficiency, a dehydration temperature of 120 °C was considered as the maximum. This is because solar boilers decrease in efficiency when the output temperature is increased. To discharge the battery, a steady supply of humid air must be provided. The proposed water supply comes from a deep borehole in which the temperature in winter is approximately 12 °C. To ensure a proper discharge in winter, the heat battery should be able to hydrate using a water supply at 10 °C, corresponding to a water vapor pressure of 12 mbar. Based on these conditions 25 out of the 563 salt hydrate reactions were considered to be suitable [4]. Considering further limiting conditions, like safety and price, K_2CO_3•1.5$H_2$0 remained as a single candidate with an energy density of 0.96 GJ/m^3 in a TCM closed heat storage system. Since then various salt hydrates from the Donkers list have been investigated, sometimes with higher energy density or other more favorable thermodynamic or kinetic properties compared to K_2CO_3, but in many cases issues like chemical stability, toxicity or price led possible candidates to be disregarded [7–14]. For a review of the state of the art of TCM performance in practical application, see Li et al. [15]

Many materials have thus been examined to fit the criteria for domestic application, both by theoretical calculations, experiments and issues for practical heat storage systems. A minimum number of cycles without degradation has not been mentioned by Donkers et al. but is an important property as well. For the purpose of the present screening besides the thermodynamic criteria, the cyclability criterion was set at a minimum of 10 cycles without significant degradation. When a material can cycle 10 times without degradation in theory it means that it would last for at least 10 years. The criteria proposed by Donkers et al. are listed in Table 1, together with the cyclability criterion set in the present study.

A class of TCM materials that has possible candidates for heat storage systems for domestic use comprises the double sulfates with a general formula of $A^{I}_2B^{II}(SO_4)_2{\cdot}nH_2O$, with A a monovalent cation and B a divalent cation. These materials were not part of the earlier surveys [4,5] and only recently a limited set of these double salts has been studied in terms of energy density by Ousaleh et al. and Marinova et al. who found rather high energy densities compared to the minimal value of 1.3 GJ/m^3 in Table 1 [7–9]. Many more of these materials are known to exist from studies outside of the scope of thermal energy storage [10–13]. A number of them have been studied as materials for latent heat storage by Voigt et al. [16] This family of materials is isostructural when considering only the hexahydrates, although the tetra- and dihydrates are also structurally similar. These materials therefore offer many opportunities for optimization of a storage material as well as insights into how the performance changes with the composition in a more general sense. Therefore, all combinations of crystals with Na^+, K^+, NH_4^+ and Cs^+ in the A-position and Co^{2+}, Cu^{2+}, Fe^{2+}, Mg^{2+}, Ni^{2+} and Zn^{2+} in the B-position were considered in the present study. These compounds were synthesized and screened for the criteria listed in Table 1. Additional criteria like the hydration temperature, the safety for people and the environment, the availability of the material and price of the material, were not considered in the present study.

2. Experimental

2.1. Crystal growth

The crystals were grown according to one of seven methods. Here we explain the most used method; the other 6 methods can be found in Appendix A. Equimolar amounts of A_2SO_4 and BSO_4 hydrates were dissolved in a minimal amount of hot water. The solution was then allowed to slowly cool to room temperature. The formed crystals were dried under vacuum after which they were washed with ethanol. The crystals were then allowed to dry in ambient air for at least 24 h before analysis was performed. The suppliers and purities of the used chemicals can be found in Appendix B.

2.2. Product properties determination

2.2.1. Structure determination

To verify that the desired phases were indeed synthesized, samples were ground and X-ray powder diffraction (XRPD) patterns were recorded using a Panalytical Empyrean diffractometer with a PIXCel-detector using Cu-Kα radiation. Two examples of the patterns compared to patterns calculated from the data base structures are shown in the Results and discussion section.

2.2.2. Energy density determination

The energy density of the salts was determined by measuring the transition enthalpies using differential scanning calorimetry (DSC) using a Mettler Toledo DSC1 with an HSS8 ceramic sensor. The DSC was calibrated using the melting of Indium. This resulted in a melting peak starting at 156.5 ± 1 °C and integration of this peak gave a ΔH of 3.26 ± 0.030 kJ/mol, which agrees with the literature values of 156.6 °C and 3.28 kJ/mol [17]. Samples of about 5 mg were ground, placed in 40 μl Al

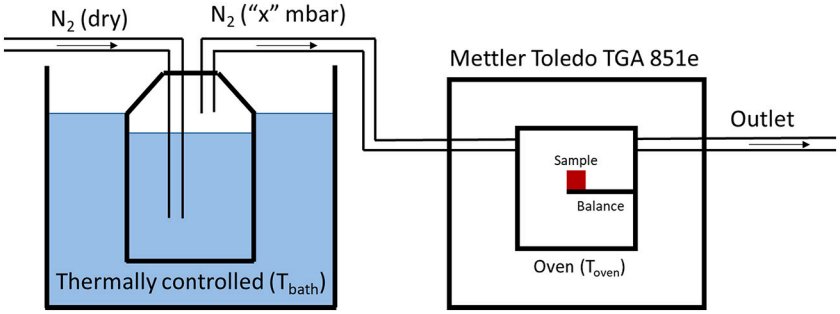


Fig. 1. Schematic representation of the equipment used for cyclability experiments; "x" is the partial water vapor pressure in the nitrogen flow, determined by the set value of T_{bath}.

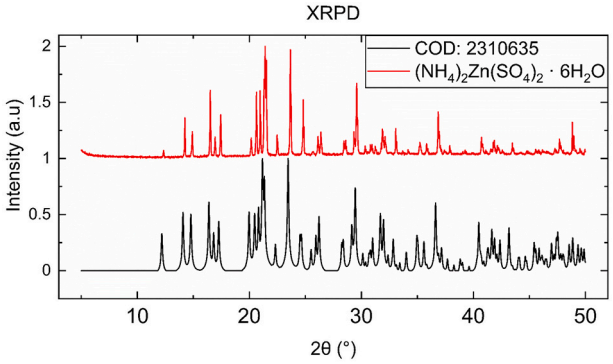


Fig. 2. X-ray powder diffractogram of $(NH_4)_2Zn(SO_4)_2{\cdot}6H_2O$.

pans, and sealed with an Al lid which was pierced right before the samples were loaded into the device. The samples were heated with 5 °C/min from 25 °C to 250 °C under a N_2 flow of 20 ml/min. For each material, three samples were measured in order to check the reproducibility.

2.2.3. Chemical stability investigation

The mass loss with increasing temperature was measured by thermogravimetric analysis (TGA) using a Mettler Toledo TGA 851^e and a Mettler Toledo TGA/DSC 3+. For these measurements, the sample material was ground and about 5 mg of sample was placed in an open 100 µl Al pan. The measurements were performed using the same temperature program as for the DSC and an N_2 flow of 20 ml/min. For each material, three samples were measured.

2.2.4. Cyclability measurements

The cyclability of the materials was determined by repeatedly cycling the temperature and recording the mass change in the Mettler Toledo TGA 851^e. To supply a steady stream of water vapor, a wash bottle filled with water was placed in a water bath which was thermally controlled. A steady N_2 flow (0.5 l/min) was led through the water in the wash bottle. This resulted in a constant water vapor pressure in the nitrogen flow determined by the set temperature of the water bath (T_{bath}). This humidified nitrogen flow was then led through the furnace/sample chamber where the sample is located. The setup is schematically depicted in Fig. 1. The water vapor pressure was calibrated by sending the humidified N_2-flow through a desiccator with an RH data logger in it (EL-USB-2 from Lascar Electronics) [18], which measured the RH for several temperatures of the water bath. All materials were cycled for 3 cycles at 22.7 ± 0.5 mbar (T_{bath} = 19 °C) water vapor pressure and when successful additional experiments were performed at 14.0 ± 0.3 mbar (T_{bath} = 10 °C) water vapor pressure. When a material could successfully cycle 3 times at this water vapor pressure, the experiment was also performed with 10 cycles to ensure chemical stability over the increased amount of cycles. The best salt was cycled 10 times also at 12 mbar water vapor pressure, i.e. the pressure from the selection criteria. All selected water vapor pressures were below the deliquescence point of the salts.

3. Results and discussion

The XRPD patterns of the synthesized materials agreed with the structures found in the ICSD or COD databases [19,20]. The database structures of all synthesized compounds are listed in Appendix C. The 24 different compounds have a monoclinic crystal structure and the $P2_1/c$ or equivalent $P2_1/a$ space group. All compounds were of high purity except for $Na_2Mg(SO_4)_2{\cdot}4H_2O$, which was slightly contaminated with $MgSO_4{\cdot}7H_2O$. The structures of all hexa-hydrates are highly similar and, for structures with the same A-ion, the XRPD patterns are almost indistinguishable. We will discuss two salts in some detail, and only give an overview of the other compounds, because of the similarities.

3.1. Results for $(NH_4)_2Zn(SO_4)_2{\cdot}6H_2O$

The XRPD of $(NH_4)_2Zn(SO_4)_2{\cdot}6H_2O$ (abbreviated to NHZnS6) in Fig. 2 shows that the pattern based on the database structure is in good agreement with the measured XRPD pattern.

The TGA graph in Fig. 3a shows that NHZnS6 loses 6 mol of water per mole salt in one single dehydration step. The dehydration reaction is as follows:

$$(NH_4)_2Zn(SO_4)_2{\cdot}6H_2O\ (s) \rightarrow (NH_4)_2Zn(SO_4)_2\ (s) + 6H_2O\ (g). \quad (1)$$

It can be seen that the reduction in sample mass in the TGA measurement coincides with the observed endothermic peak in the DSC measurement (Fig. 3b) confirming that the endothermic peak observed in the DSC measurement corresponds to the dehydration reaction. The enthalpy of dehydration is 933 ± 44 J/g which is determined from the DSC measurement. This amounts to an energy density of 1.78 GJ/m^3 of the hydrated salt which is well above the energy density criteria set by Donkers et al. in Table 1 [4]. The onset of the dehydration reaction is at 92.5 ± 3.0 °C. Fig. 3 shows the results of three samples and this demonstrates a good reproducibility. The anhydrate is stable until at least

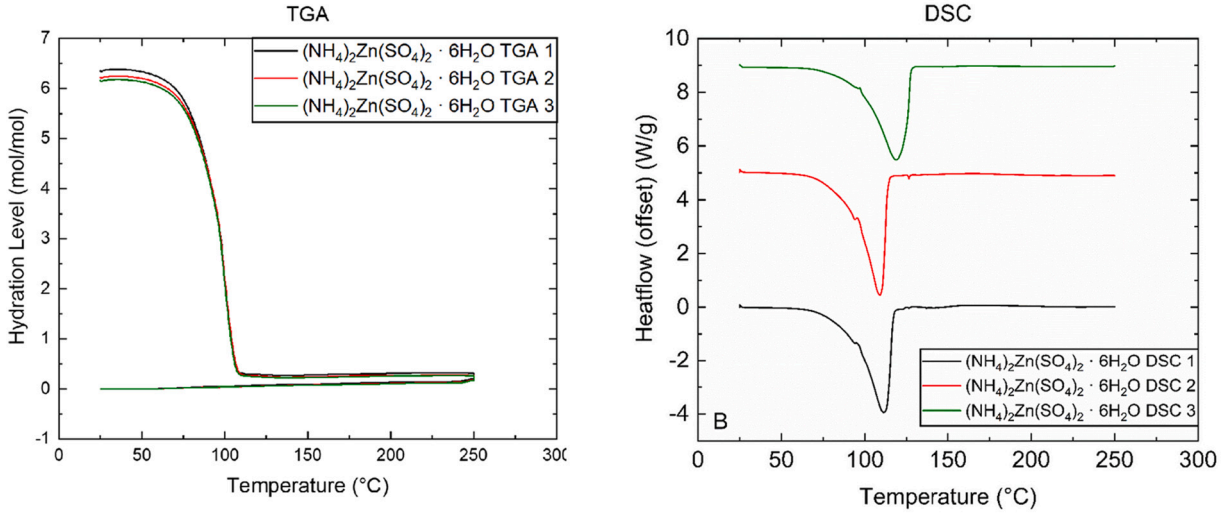


Fig. 3. (a) Thermogravimetric analysis of $(NH_4)_2Zn(SO_4)_2{\cdot}6H_2O$ in triplo. (b) Differential scanning calorimetry measurement of $(NH_4)_2Zn(SO_4)_2{\cdot}6H_2O$ in triplo.

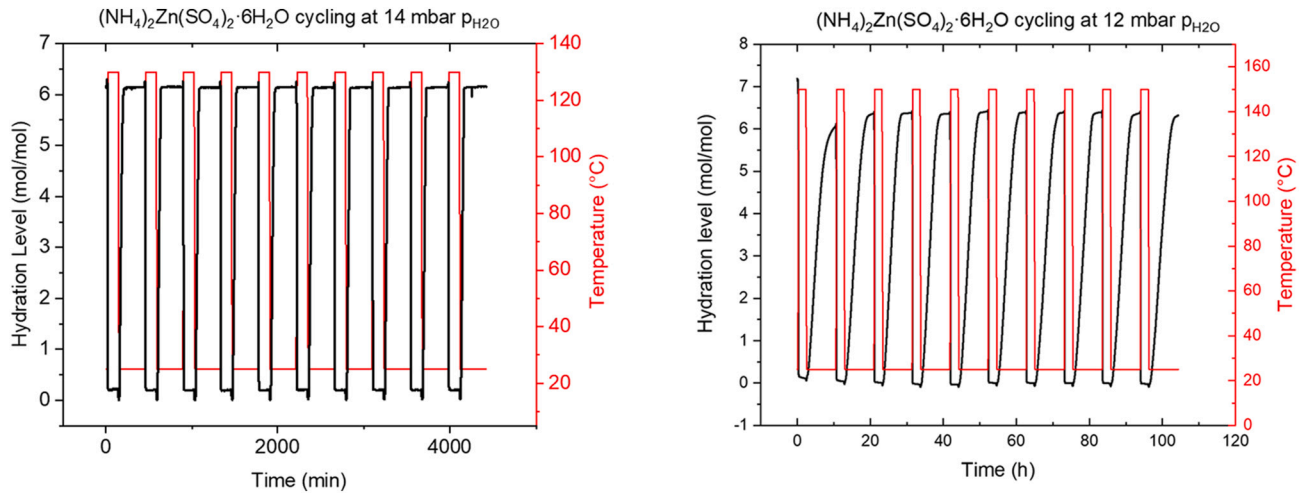


Fig. 4. $(NH_4)_2Zn(SO_4)_2{\cdot}6H_2O$ is dehydrated and hydrated in cycles for a total of 10 cycles at both 14 (left) and 12 mbar (right). The left axis (black) shows the hydration level, while the right axis (red) shows the temperature program in degrees Celsius.

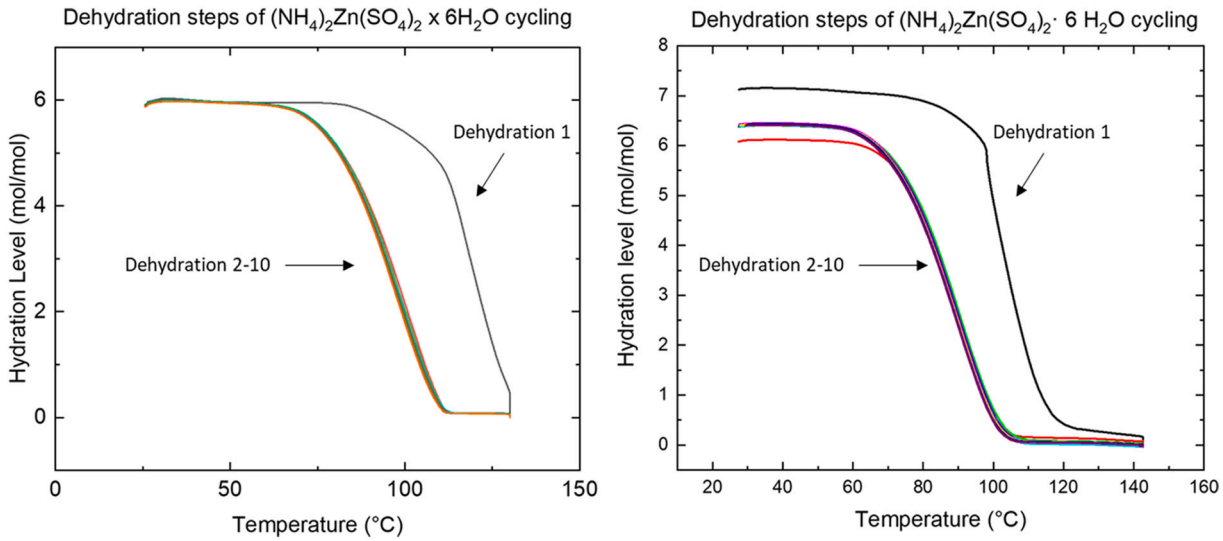


Fig. 5. Dehydration steps of the 10 times cycling experiment shown in Fig. 4 at 14 (left) and 12 mbar (right). Dehydration step 1 clearly occurs at a higher temperature than the subsequent dehydrations for both water vapor pressures.

250 °C; this is noteworthy because for all other ammonium-based salts that were analyzed an additional mass loss was observed at temperatures higher than 200 °C. This mass loss is most likely due to the loss of one of the ammonia molecules.

The cycling of NHZnS6 is shown in Fig. 4. NHZnS6 was dehydrated and hydrated for a total of 10 cycles at both 14 (left) and 12 mbar (right). The left axis (black) shows the hydration level, while the right axis (red) shows the temperature program in degrees Celsius. The temperature was cycled between 25 and 130 °C at a water vapor pressure of 14 mbar (10 °C wash bottle) and between 25 and 150 °C at a water vapor pressure of 12 mbar. It can be observed that the compound loses and gains 6 mol of water in each cycle and that there is no degradation of the material after 10 cycles. In Fig. 5 the same experiments are shown but plotted versus temperature to illustrate the evolution of the dehydration. It demonstrates that the first dehydration step occurs at a higher temperature than all consecutive ones. This is not unusual as the material tends to crack in the first (few) cycle(s) until a sufficiently porous structure is reached that can hydrate/dehydrate without significant change [21]. As cyclability at 14 mbar was successful, cyclability at 12 mbar was also tested, shown in Figs. 4 and 5 on the right. This revealed that NHZnS6 can cycle 10 times at 12 mbar although it requires a longer hydration time (8 h instead of 5).

The energy density of NHZnS6 has also been measured after 1 and 10 dehydration-hydration cycles to ensure that the enthalpy of dehydration remains the same after the structural changes. Results show that after the first dehydration-hydration cycle NHZnS6 has an enthalpy of dehydration of 957 ± 23 J/g and after 10 cycles the enthalpy is 891 J/g. Both are within the error margin of the non-cycled compound. The dehydration temperature was, however, lowered to 84.2 ± 1.7 °C after the first dehydration, which was significantly lower than the dehydration temperature of the non-cycled compound. This agrees with our cycling measurements, and, as stated earlier, is attributed to the changing porosity of the material. As explained in the introduction, the lower the required output temperature of the solar boiler, the more efficient it can perform. A lowering of the dehydration temperature after a first cycle is therefore beneficial for the application.

The energy density, dehydration temperature and hydration water vapor pressure fulfill the criteria set by Donkers [4]. On top of that NHZnS6 shows no sign of chemical degradation after 10 cycles.

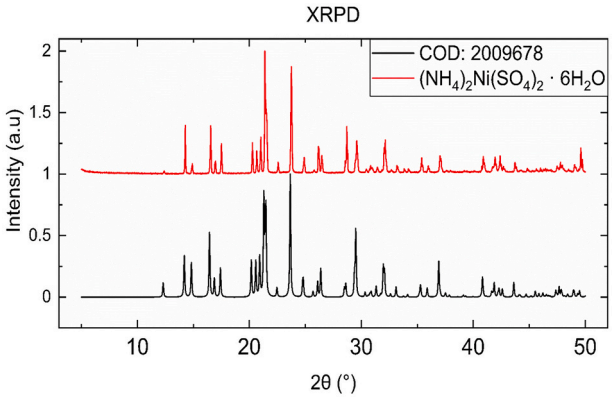


Fig. 6. X-Ray Powder Diffraction of $(NH_4)_2Ni(SO_4)_2{\cdot}6H_2O$.

3.2. Results for $(NH_4)_2Ni(SO_4)_2{\cdot}6H2O$

$(NH_4)_2Ni(SO_4)_2{\cdot}6H_2O$ (abbreviated as NHNiS6) was successfully grown from solution, which is confirmed by the XRPD pattern shown in Fig. 6. The dehydration profile of NHNiS6 is illustrated in Fig. 7a. NHNiS6 has a single dehydration step of 6 mol water per mole salt after which one additional mole is apparently lost slowly over time. Because ammonia and water have a similar mass, this additional loss of 1 mol can be explained by the loss of an ammonia molecule. The dehydration reaction is as follows:

$$(NH_4)_2Ni(SO_4)_2{\cdot}6H_2O\ (s) \rightarrow (NH_4)_2Ni(SO_4)_2\ (s) + 6H_2O\ (g). \quad (2)$$

The loss of an ammonia molecule is expected to be as follows:

$$(NH_4)_2Ni(SO_4)_2\ (s) \rightarrow NH_4Ni(HSO_4)(SO_4)\ (s) + NH_3\ (g). \quad (3)$$

NHNiS6 has an enthalpy of dehydration of 942 ± 25 J/g as determined from the DSC measurements shown in Fig. 7b. The enthalpy of dehydration corresponds to an energy density of 1.80 GJ/m^3. The onset for the dehydration reaction is at 132.4 ± 3.1 °C. The energy density passes the criteria, but the dehydration onset temperature is too high by 12°.

The cycling experiment of NHNiS6 is shown in Fig. 8 for temperature cycles were 25 and 150 °C and a water vapor pressure over the sample of 14 mbar (10 °C wash bottle). At this temperature, the material roughly cycles 5.5 mol water per mole salt for the full 10 cycles. When the material was cycled with a maximum cycle temperature of 180 °C (Fig. S21) instead of 150 °C, it was observed that the material started to cycle with

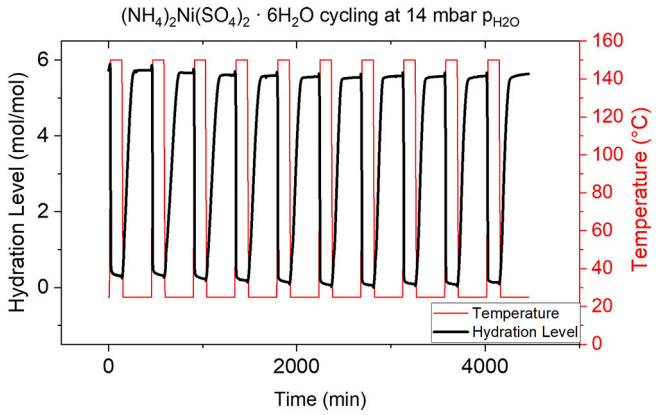


Fig. 8. $(NH_4)_2Ni(SO_4)_2{\cdot}6H_2O$ is dehydrated and hydrated in cycles for a total of 10 cycles. The left axis (black) shows the hydration level, while the right axis (red) shows the temperature program in degrees Celsius. (For interpretation of the references to colour in this figure legend, the reader is referred to the web version of this article.)

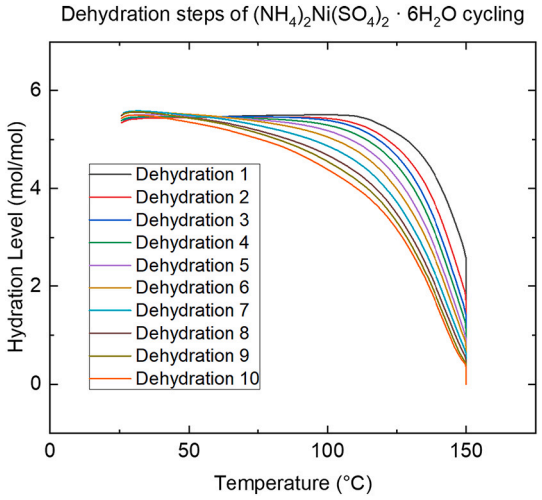
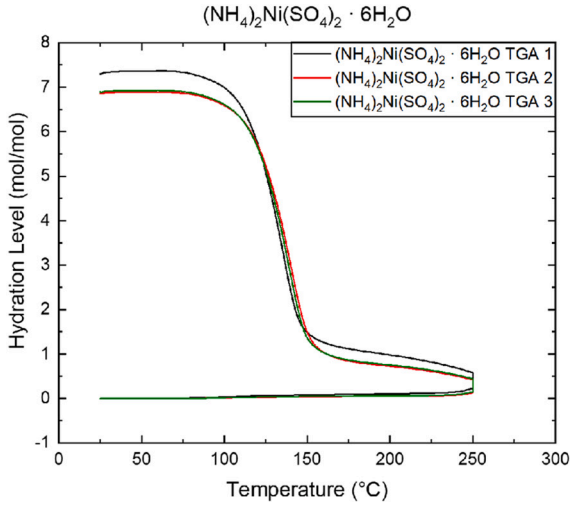


Fig. 9. Dehydration steps of the 10 times cycling experiment shown in Fig. 8. The dehydration temperature gradually decreases over the 10 cycles.



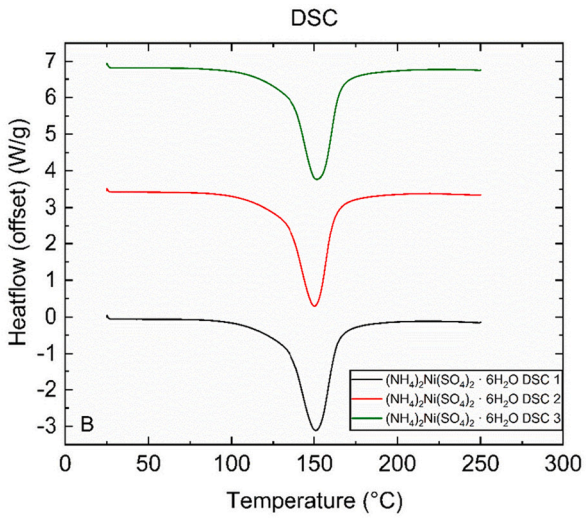


Fig. 7. (a) Thermogravimetric analysis of $(NH_4)_2Ni(SO_4)_2$ $6H_2O$ in triplo. (b) Differential scanning calorimetry measurement of $(NH_4)_2Ni(SO_4)_2{\cdot}6H_2O$ in triplo.

Table 2
A list of the important parameters for all double salts investigated. The values that pass the set criteria are in bold. If a Compound has multiple dehydration phases, all are listed with the corresponding energies of the separate peaks between brackets. The values are given with a 95 % confidence interval.

Compound	Onset/dehydration temperature (°C)	Total energy (J/g)	Enthalpy (kJ/mol H_2O)	Total energy density (GJ/m^3)	Cyclability at $P_{H2O} \leq$ 14 mbar $T_{bath} = 10$ °C	Comments
$Na_2Co(SO_4)_2{\cdot}4H_2O$	153 ± 0.3	583 ± 36	54 ± 3	**1.43**	No	Overlapping two phase dehydration
$Na_2Cu(SO_4)_2{\cdot}2H_2O$	185 ± 1	413 ± 18	70 ± 3	1.20	No	
$Na_2Fe(SO_4)_2{\cdot}4H_2O$	137 ± 0.5	485 ± 30	44 ± 3	1.17	No	
$Na_2Mg(SO_4)_2{\cdot}4H_2O$	**118 ± 0.03** 198 ± 3	668 ± 29 (304), (364)	56 ± 2	**1.49**	No	$Mg(SO_4)\cdot 7H_2O$ contamination, Two phase dehydration
$Na_2Ni(SO_4)_2{\cdot}4H_2O$	180 ± 0.5	697 ± 35	64 ± 3	**1.74**	No	Overlapping two phase dehydration
$Na_2Zn(SO_4)_2{\cdot}4H_2O$	**112 ± 1** 128 ± 2	643 ± 22 (310), (333)	60 ± 2	**1.62**	No	Two phase dehydration
$K_2Co(SO_4)_2{\cdot}6H_2O$	**108 ± 6**	838 ± 10	61 ± 1	**1.85**	No	
$K_2Cu(SO_4)_2{\cdot}6H_2O$	**62 ± 1** 138 ± 0.1	872 ± 18 (563), (309)	64 ± 1	**1.97**	No	Two phase dehydration
$K_2Fe(SO_4)_2{\cdot}6H_2O$	**59 ± 2** **93 ± 1** 156 ± 0.1	525 ± 26 (6), (236), (283)	38 ± 2	1.13	No	Three phase dehydration Dehydration in air prior to measurement
$K_2Mg(SO_4)_2{\cdot}6H_2O$	–	885 ± 8	59 ± 2	**1.81**	No	Peak shapes differ within triplo
$K_2Ni(SO_4)_2{\cdot}6H_2O$	137 ± 3	796 ± 49	57 ± 1	**1.78**	No	
$K_2Zn(SO_4)_2{\cdot}6H_2O$	**105 ± 0.3**	801 ± 33	63 ± 1	**1.79**	No	
$(NH_4)_2Co(SO_4)_2{\cdot}6H_2O$	**106 ± 1**	860 ± 22	55 ± 1	**1.63**	No	
$(NH_4)_2Cu(SO_4)_2{\cdot}6H_2O$	**75 ± 6**	943 ± 11	61 ± 3	**1.81**	No	Overlapping Two phase dehydration
$(NH_4)_2Fe(SO_4)_2{\cdot}6H_2O$	**102 ± 4**	847 ± 14	55 ± 1	**1.61**	No	
$(NH_4)_2Mg(SO_4)_2{\cdot}6H_2O$	**106 ± 3**	1021 ± 49	61 ± 3	**1.75**	No	
$(NH_4)_2Ni(SO_4)_2{\cdot}6H_2O$	132 ± 3	942 ± 25	62 ± 2	**1.80**	**Yes**	
$(NH_4)_2Zn(SO_4)_2{\cdot}6H_2O$	**93 ± 3**	933 ± 44	62 ± 3	**1.78**	**Yes**	
$Cs_2Co(SO_4)_2{\cdot}6H_2O$	**101 ± 1**	602 ± 37	63 ± 4	**1.72**	No	
$Cs_2Cu(SO_4)_2{\cdot}6H_2O$	**89 ± 2** 173 ± 1	472 ± 13	50 ± 1	**1.33**	No	Three phase dehydration with first two overlapping
$Cs_2Fe(SO_4)_2{\cdot}6H_2O$	95 ± 1	579 ± 8	60 ± 1	**1.62**	No	Overlapping Two phase dehydration
$Cs_2Mg(SO_4)_2{\cdot}6H_2O$	55 ± 2	644 ± 16	63 ± 2	**1.73**	No	Overlapping two phase dehydration
$Cs_2Ni(SO_4)_2{\cdot}6H_2O$	123 ± 4	611 ± 39	64 ± 4	**1.76**	No	
$Cs_2Zn(SO_4)_2{\cdot}6H_2O$	**82 ± 4**	602 ± 7	63 ± 1	**1.73**	No	

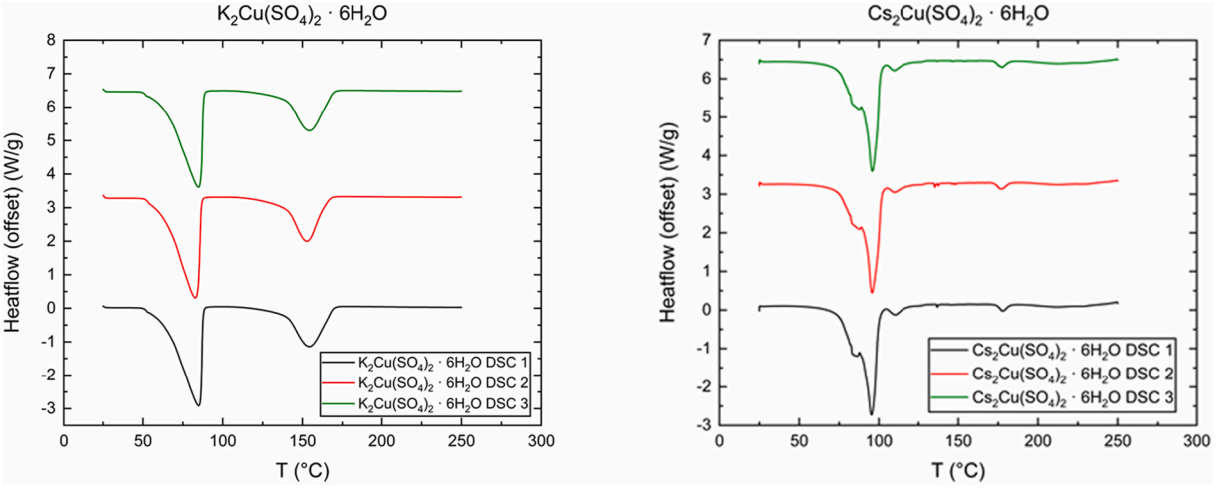


Fig. 10. DSC results of $K_2Cu(SO_4)_2{\cdot}6H_2O$ and $Cs_2Cu(SO_4)_2{\cdot}6H_2O$ each showing several dehydration peaks which overlap for $Cs_2Cu(SO_4)_2{\cdot}6H_2O$.

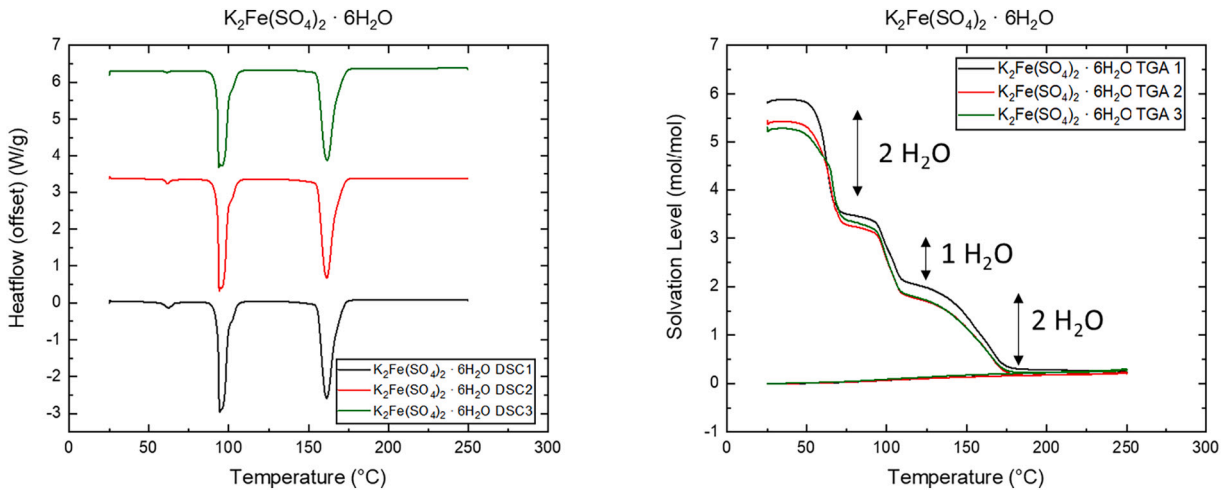


Fig. 11. DSC (left) and TGA (right) results of $K_2Fe(SO_4)_2$. Both DSC and TGA show three transitions.

fewer moles of water, which indicates the degradation of the material. This might be due to a slow evaporation of the NH_3 from the compound at high temperatures, altering its structure in a way that it cannot rehydrate. However, when the material is not heated too far above the dehydration temperature this should not be a problem.

In Fig. 9 it can be seen that the dehydration temperature of the material gradually decreases over the 10 cycles. It is unknown after how many cycles the material attains a stable porous structure and the decrease in dehydration temperature stops. It is imaginable that the decrease in dehydration temperature causes NHNiS6 to pass the dehydration temperature criteria. If this is the case than NHNiS6 is also a viable option as TCM, but this requires further investigation.

3.3. Overview all double salts

In Table 2 an overview of all double salts studied is given. All the DSC, TGA and cycle experiments on which Table 2 is based can be found in the supporting information. In general, the large A – ions can form hexahydrates and smaller A – ions like sodium only seem to form di- and tetra-hydrates while Li based double sulfate salts do not form hydrates at all according to the literature [22,23]. The trend that can be observed is that the larger the A–ion the more water molecules can be placed within the double salt hydrate structure. 21 out of 24 salts have passed the energy density criteria which shows that this family of salts has the potential for good TCM's. Some of the materials have two dehydration phases which can be observed as two separate peaks in the DSC data, for example shown in the DSC result of $K_2Cu(SO_4)_2{\cdot}6H_2O$ in Fig. 10 (left). It is often the case that two dehydration phases overlap, for example shown in the DSC result of $Cs_2Cu(SO_4)_2{\cdot}6H_2O$ in Fig. 10 (right), and in these cases the onset temperature of the first peak was noted. Overlapping or merged peaks can be separated by lowering the scanning rate of the DSC measurement.

3.3.1. Enthalpies

The heat of vaporization of liquid water is about 40 kJ/mol at the temperatures we are considering here. Most salts investigated show enthalpies of 50 to 70 kJ/mol H_2O, meaning that the bonding of the water in the crystal structure is stronger than in liquid water, but the enthalpies for $Na_2Fe(SO_4)_2$ and $K_2Fe(SO_4)_2$, respectively 44 ± 3 and 38 ± 2 kJ/mol, are relatively low. This means the water is not strongly bound in these compounds, but why that is the case is hard to tell. DFT calculations could be one way to tackle this, but are beyond the scope of this paper. We have not found a clear dependence on the specific compound; e.g. several of the Fe-containing salts have normal values. For the case of $K_2Fe(SO_4)_2$ part of the low enthalpy could be due to dehydration in air between sample preparation and the measurement while a hydration state of 6 was assumed. This is supported by the TGA result, shown in Fig. 11 right, since it starts dehydration at 5 mol/mol instead of 6 mol H_2O. It could also explain the very small peak for the first dehydration step at 59 °C in the DSC result, Fig. 11 left, suggesting that the first 2 mol of H_2O released are weakly bound in the crystal structure.

Table 3
Comparison energy densities literature vs. measured.

Compound	Energy density Ousaleh [7] (GJ/m^3)	Energy density measured (GJ/m^3)
$Na_2Zn(SO_4)_2{\cdot}4H_2O$	4.7	1.62
$Na_2Mg(SO_4)_2{\cdot}4H_2O$	5.5	1.49
$Na_2Cu(SO_4)_2{\cdot}2H_2O$	3.2	1.20

3.3.2. Sodium salts

The sodium double sulfates were previously investigated by Ousaleh et al. [7]. Their reported energy densities are given in Table 3. From the table it can be seen that the energy densities that were measured in the present research are approximately 3 times lower.

The DSC apparatus correctly measured the energy density of the well-known $K_2CO_3{\cdot}1.5H_2O$, making an experimental error unlikely [24]. Multiple experimental parameters like: the nitrogen flow, temperature program and the sample container have been varied to explain this large difference, but the cause of this difference remains unclear. The method for cycling experiments employed by Ousaleh et al. is not fully documented and therefore not reproducible. The sodium salts overall have dehydration temperatures above 120 °C and do not completely hydrate again after dehydration even when a water vapor pressure of 22.7 mbar is applied.

3.3.3. Potassium salts

The potassium salts are not suitable because they do not pass the cyclability requirements. This is because they don't fully hydrate after the first dehydration step, not even at 22.7 mbar water vapor pressure. This is likely due to kinetics, since the salts do start to hydrate and prior dehydration experiments with TGA do not show any weight loss other than the expected mass loss corresponding to 6 mol of H_2O. For $K_2Mg(SO_4)_2{\cdot}6H_2O$ there were different peak patterns between the triplo DSC measurements. The total energy of the different experiments was equivalent, however.

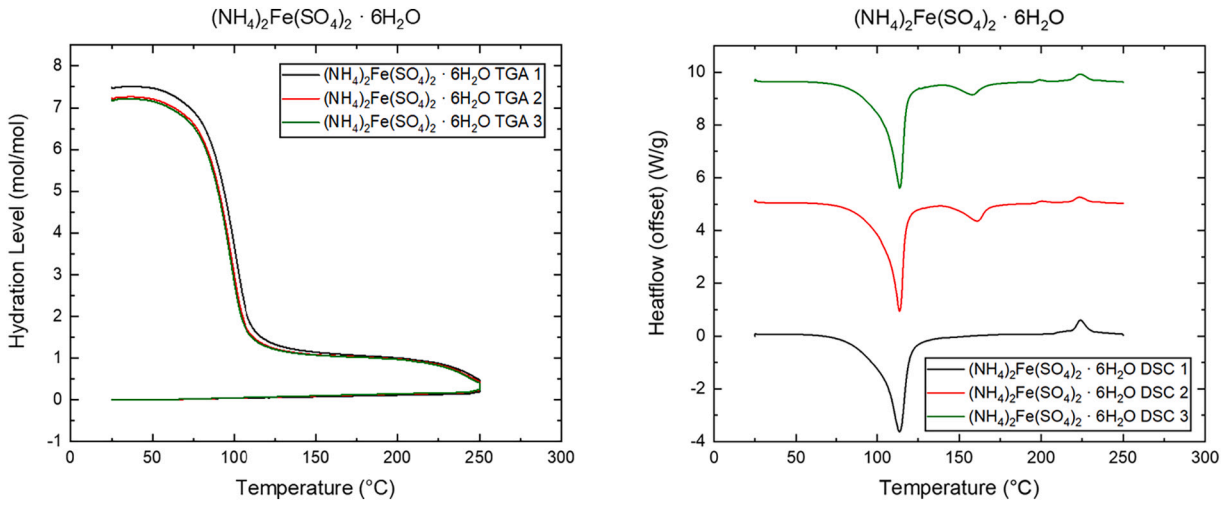


Fig. 12. TGA and DSC results of dehydration of $(NH_4)_2Fe(SO_4)_2{\cdot}6H_2O$.

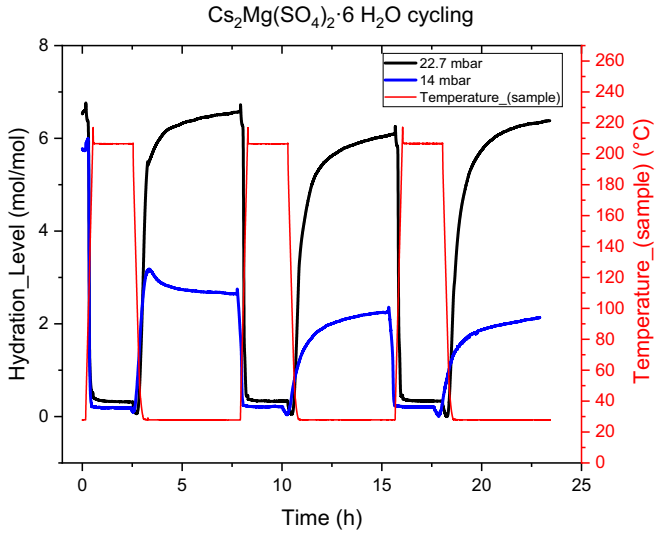


Fig. 13. Cyclability of $Cs_2Mg(SO_4)_2$ at both 22.7 (in black) and 14 mbar (in blue). (For interpretation of the references to colour in this figure legend, the reader is referred to the web version of this article.)

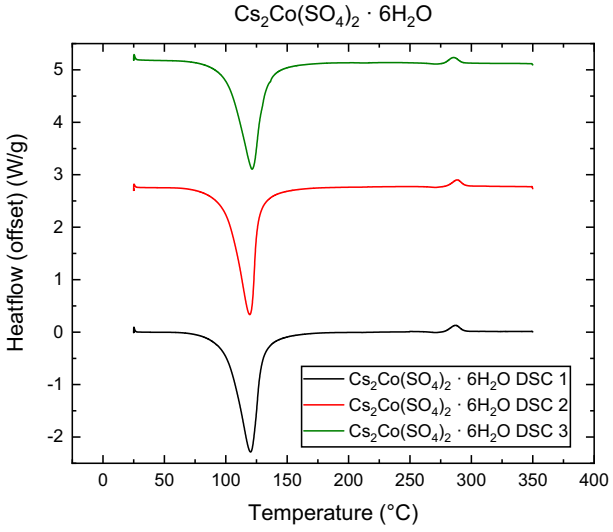


Fig. 14. DSC result of dehydration of $Cs_2Co(SO_4)_2$ with an exothermic peak around 280 °C.

3.3.4. *Ammonium salts*

The ammonium salts are the most promising of all salts because they all have a sufficient energy density and almost all of them dehydrate below 120 °C. It is found that $(NH_4)_2Cu(SO_4)_2{\cdot}6H_2O$ is not cyclable. $(NH_4)_2Mg(SO_4)_2{\cdot}6H_2O$ and $(NH_4)_2Fe(SO_4)_2{\cdot}6H_2O$ are cyclable at a water vapor pressure of 22.7 mbar. $(NH_4)_2Zn(SO_4)_2{\cdot}6H_2O$ and $(NH_4)_2Ni(SO_4)_2{\cdot}6H_2O$ can cycle at water vapor pressures of 22.7 and 14 mbar. All the ammonium salts except for $(NH_4)_2Zn(SO_4)_2{\cdot}6H_2O$ lose additional mass after full dehydration at temperatures above 200 °C. This is an exothermic process likely caused by the formation and loss of an ammonia molecule. This process is demonstrated for $(NH_4)_2Fe(SO_4)_2{\cdot}6H_2O$ in Fig. 12. It shows an exothermic peak at 220 °C of 20 J/g.

3.3.5. *Cesium salts*

All of the cesium double salts have a proper energy density and sufficiently low dehydration temperature. However, all cesium salts failed on the cyclability criterium because they did not fully cycle at a water vapor pressure of 14 mbar, although $Cs_2Mg(SO_4)_2$ and $Cs_2Ni(SO_4)_2$ did cycle at a water vapor pressure of 22.7 mbar indicating a kinetic issue for the hydration at lower water vapor pressures. The cyclability at 22.7 and 14 mbar of $Cs_2Mg(SO_4)_2$ is shown in Fig. 13. $Cs_2Co(SO_4)_2$ shows an exothermic peak of 12 ± 4 J/g in the DSC result, shown in Fig. 14 at 279 ± 2.7 °C, indicating that some chemical reaction, potentially degradation, is happening.

4. Conclusion

Synthesis of all 24 double salts was successful as confirmed by the XRPD patterns. DSC and TGA analyses were performed on all synthesized materials. Most of the synthesized materials do not fit the criteria set for residential use but do possess interesting properties that can be explored with the mixing of these double sulfate salts. $(NH_4)_2Fe(SO_4)_2{\cdot}6H_2O$, $(NH_4)_2Mg(SO_4)_2{\cdot}6H_2O$, $Cs_2Mg(SO_4)_2{\cdot}6H_2O$ and $Cs_2Ni(SO_4)_2{\cdot}6H_2O$ fulfill the energy density and dehydration temperature criteria, but they require 22.7 mbar to achieve cyclability. $(NH_4)_2Ni(SO_4)_2{\cdot}6H_2O$ is a possible heat storage candidate because it cycles properly at a $P_{H2O} = 14$ mbar although the dehydration temperature is too high to be suitable for residential use. $(NH_4)_2Zn(SO_4)_2{\cdot}6H_2O$ has an energy density of 1.78 GJ/m^3, a dehydration temperature of 84 °C after 1 cycle and is fully cyclable for at least 10 cycles at both 14 and 12 mbar without loss of performance. $(NH_4)_2Zn(SO_4)_2{\cdot}6H_2O$ is thus the most

promising candidate for thermochemical heat storage application, the more as it is low-cost, abundantly available and safe. Therefore, the compound should be further investigated in applications as a thermochemical material.

CRediT authorship contribution statement

W. Kooijman: Investigation, Formal analysis, Writing – original draft. **D.J. Kok:** Conceptualization, Writing – original draft, Writing – review & editing. **M.A.R. Blijlevens:** Supervision, Writing – review & editing. **H. Meekes:** Supervision, Writing – review & editing. **E. Vlieg:** Supervision, Writing – review & editing.

Declaration of competing interest

The authors declare that they have no known competing financial interests or personal relationships that could have appeared to influence the work reported in this paper.

Data availability

Data will be made available on request.

Acknowledgements

Part of this research was funded by the Dutch Research Council (NWO) in the framework of Materials for Sustainability through the Materials for Heat Storage project.

Appendix A

Table 4 shows the growth method labeled by numbers 1–7 used for each double sulfate hydrate.

Table 4
Growth methods used for the various compounds; labels refer to the methods listed below.

A-ion↓\B-ion →	Co^{2+}	Cu^{2+}	Fe^{2+}	Mg^{2+}	Ni^{2+}	Zn^{2+}
Na^+	3	3	4	7	3	5
K^+	1	1	2	6	1	1
NH_4^+	1	1	2	1	1	1
Cs+	1	1	2	1	1	1

1. Equimolar amounts of A_2SO_4 and BSO_4 hydrates were dissolved in a minimal amount of hot water. The solution was then allowed to slowly cool to room temperature. Upon cooling down crystals formed. These crystals were dried under vacuum after which they were washed with ethanol. The crystals were then allowed to dry in ambient air for at least 24 h.
2. Equimolar amounts of A_2SO_4 and BSO_4 hydrates were dissolved in a minimal amount of hot 5 mM sulfuric acid to prevent the oxidation of Fe^{2+} to Fe^{3+} [25]. The solution was then allowed to slowly cool to room temperature. During cooling down crystals formed. These crystals were dried under vacuum after which they were washed with ethanol. The crystals were then allowed to dry in ambient air for at least 24 h.
3. Equimolar amounts of ASO_4 and BSO_4 hydrates were dissolved in a minimal amount of water and crystals were grown by slowly evaporating the solvent at room temperature. These crystals were dried under vacuum and washed with ethanol. The crystals were then allowed to dry in ambient air for at least 24 h.
4. Equimolar amounts of A_2SO_4 and BSO_4 hydrates were suspended in 5 mM sulfuric acid to prevent the oxidation of Fe^{2+} to Fe^{3+} [25]. The suspension was stirred for 24 h after which it was filtered under vacuum and washed with ethanol. The resulting powder was then allowed to dry in ambient air for at least 24 h
5. Equimolar amounts of A_2SO_4 and BSO_4 hydrates were suspended in water. The suspension was stirred for 24 h after which it was filtered under vacuum and washed with ethanol. The resulting powder was then allowed to dry in ambient air for at least 24 h
6. A 1:3 molar ratio of A_2SO_4 and BSO_4 hydrates was dissolved in a minimal amount of water. The solvent was allowed to slowly evaporate at room temperature, which caused crystals to form. These crystals were dried under vacuum and they were subsequently dried in ambient air for at least 24 h.
7. A 1:3 molar ratio of A_2SO_4 and BSO_4 hydrates was suspended in water. The suspension was stirred for 24 h. The suspension was dried under vacuum and the resulting powder was subsequently dried in ambient air for at least 24 h.

Appendix B

Table 5
The suppliers and purities of the used chemicals.

Substance	Supplier	Grade/purity
$(NH_4)_2SO_4$	J.T. Baker	99 % Analysis grade
$CoSO_4{\cdot}7H_2O$	Sigma-Aldrich	99 % Reagent plus
$CuSO_4{\cdot}5H_2O$	Sigma-Aldrich	98 % ACS Reagent
Cs_2SO_4	Sigma Aldrich	99.99 % trace metal basis
$FeSO_4{\cdot}7H_2O$	Merck	99 % Analysis grade
$MgSO_4$	Acros Organics	99 % Extra pure
$NiSO_4{\cdot}6H_2O$	Merck	99 % Analysis grade
Na_2SO_4	Merck	99 % Analysis grade

(*continued on next page*)

Table 5 (*continued*)

Substance	Supplier	Grade/purity
K_2SO_4	Merck	99 % Analysis grade
Sulfuric acid	Merck	95–97 % Analysis grade
$ZnSO_4{\cdot}7H_2O$	Sigma Aldrich	99.0 % analysis grade

Appendix C

Table 6
The database structures and space groups of all synthesized compounds [19,20].

Compound	Database	Space group
$Na_2Co(SO_4)_2{\cdot}4H_2O$	ICSD:267442	P $2_1/c$
$Na_2Cu(SO_4)_2{\cdot}2H_2O$	COD:9007608	P $2_1/c$
$Na_2Fe(SO_4)_2{\cdot}4H_2O$	COD:2217413	P $2_1/c$
$Na_2Mg(SO_4)_2{\cdot}4H_2O$	COD:2008059	P $2_1/a$
$Na_2Ni(SO_4)_2{\cdot}4H_2O$	COD:2210317	P $2_1/c$
$Na_2Zn(SO_4)_2{\cdot}4H_2O$	COD:9011018	P $2_1/a$
$K_2Co(SO_4)_2{\cdot}6H_2O$	COD:9013503	P $2_1/a$
$K_2Cu(SO_4)_2{\cdot}6H_2O$	COD:4343907	P $2_1/a$
$K_2Fe(SO_4)_2{\cdot}6H_2O$	COD:2208450	P $2_1/a$
$K_2Mg(SO_4)_2{\cdot}6H_2O$	COD:9008113	P $2_1/a$
$K_2Ni(SO_4)_2{\cdot}6H_2O$	COD:9013504	P $2_1/a$
$K_2Zn(SO_4)_2{\cdot}6H_2O$	COD:9013506	P $2_1/a$
$(NH4)_2Co(SO_4)_2{\cdot}6H_2O$	COD:2204139	P $2_1/c$
$(NH4)_2Cu(SO_4)_2{\cdot}6H_2O$	COD:2019135	P $2_1/c$
$(NH4)_2Fe(SO_4)_2{\cdot}6H_2O$	COD:9011369	P $2_1/a$
$(NH4)_2Mg(SO_4)_2{\cdot}6H_2O$	COD:9008087	P $2_1/a$
$(NH4)_2Ni(SO_4)_2{\cdot}6H_2O$	COD:2009678	P $2_1/c$
$(NH4)_2Zn(SO_4)_2{\cdot}6H_2O$	COD:2310635	P $2_1/a$
$Cs_2Co(SO_4)_2{\cdot}6H_2O$	COD:8100509	P $2_1/a$
$Cs_2Cu(SO_4)_2{\cdot}6H_2O$	COD:1541871	P $2_1/a$
$Cs_2Fe(SO_4)_2{\cdot}6H_2O$	COD:8100508	P $2_1/a$
$Cs_2Mg(SO_4)_2{\cdot}6H_2O$	COD:8100506	P $2_1/a$
$Cs_2Ni(SO_4)_2{\cdot}6H_2O$	COD:8100510	P $2_1/a$
$Cs_2Zn(SO_4)_2{\cdot}6H_2O$	COD:8100511	P $2_1/a$

Appendix D. Supplementary data

Supplementary data to this article can be found online at https://doi.org/10.1016/j.est.2022.105459.

References

[1] Eurostat, Disaggregated final energy consumption in households - quantities. https://ec.europa.eu/eurostat/databrowser/view/nrg_d_hhq/default/table?lang=en (accessed 2021-09-10).
[2] F. Belaïd, Understanding the spectrum of domestic energy consumption: empirical evidence from France, Energy Policy 92 (2016) 220–233.
[3] M. Deutsch, D. Müller, C. Aumeyr, C. Jordan, C. Gierl-Mayer, P. Weinberger, F. Winter, A. Werner, Systematic search algorithm for potential thermochemical energy storage systems, Appl. Energy 183 (2016) 113–120.
[4] P.A.J. Donkers, L.C. Sögütoglu, H.P. Huinink, H.R. Fischer, O.C.G. Adan, A review of salt hydrates for seasonal heat storage in domestic applications, Appl. Energy 199 (2017) 45–68.
[5] D. Aydin, S.P. Casey, S. Riffat, The latest advancements on thermochemical heat storage systems, Renew. Sustain. Energy Rev. 41 (2015) 356–367.
[6] A. de Jong, F. Trausel, C. Finck, L. van Vliet, R. Cuypers, Thermochemical heat storage – system design issues, Energy Procedia 48 (2014) 309–319.
[7] H. Ait Ousaleh, S. Sair, A. Zaki, A. Faik, J. Mirena Igartua, A. El Bouari, Double hydrates salt as sustainable thermochemical energy storage materials: evaluation of dehydration behavior and structural phase transition reversibility, Sol. Energy 201 (2020) 846–856.
[8] D. Marinova, M. Georgiev, T. Bancheva, D. Stoilova, On the formation of solid solutions with blödite-and kröhnkite-type structures. II. Structural and thermal investigations of solid solutions Na2Zn1–xCux (SO4) 2· 4H2O (0< x< 0.14), Int. J. Sci. Res. Sci. Technol. 2 (2016) 283–295.
[9] H. Ait Ousaleh, S. Sair, A. Zaki, A. Younes, A. Faik, A. El Bouari, Advanced experimental investigation of double hydrated salts and their composite for improved cycling stability and metal compatibility for long-term heat storage technologies, Renew. Energy 162 (2020) 447–457.
[10] V.L. Manomenova, E.B. Rudneva, A.E. Voloshin, Crystals of the simple and complex nickel and cobalt sulfates as optical filters for the solar-blind technology, Russ. Chem. Rev. 85 (6) (2016) 585–609.
[11] S. Ghosh, M. Oliveira, T.S. Pacheco, G.J. Perpetuo, C.J. Franco, Growth and characterization of ammonium nickel-cobalt sulfateTutton's salt for UV light applications, J. Cryst. Growth 487 (2018) 104–115.
[12] S.D. Binitha, V.T. Jisha, Preparation and antibacterial characteristics of mixed crystals of tutton salt (NH4)KZn(SO4)2. 6H2O, J. Adv. Sci. Res. 12 (2021) 111–116.
[13] V.M. Kovrugin, D.O. Nekrasova, O.I. Siidra, O. Mentré, C. Masquelier, S. Y. Stefanovich, M. Colmont, Mineral-inspired crystal growth and physical properties of Na2Cu(SO4)2 and review of Na2M(SO4)2(H2O)x (x = 0–6) compounds, Cryst. Growth Des. 19 (2) (2019) 1233–1244.
[14] F. Desai, S.P. Jenne, P. Muthukumar, M.M. Rahman, Thermochemical energy storage system for cooling and process heating applications: a review, Energy Convers. Manag. 229 (2021).
[15] W. Li, J.J. Klemes, Q.W. Wang, M. Zeng, Salt hydrate-based gas-solid thermochemical energy storage: current progress, challenges, and perspectives, Renew. Sustain. Energy Rev. 154 (2022).
[16] W. Voigt, S. Göring, Melting of Tutton's salts studied by DSC, Thermochim. Acta 237 (1) (1994) 13–26.
[17] J.A. Dean, Lange's Handbook of Chemistry, Fifteenth ed., McGraw-Hill, Inc., 1999.
[18] electronics, L. Easylog EL-USB-2: temperature and relative humidity USB data logger. https://www.lascarelectronics.com/easylog-el-usb-2 (accessed 2021-09-10).
[19] G. Bergerhoff, R. Hundt, R. Sievers, I.D. Brown, The inorganic crystal-structure data-base, J. Chem. Inf. Comput. Sci. 23 (2) (1983) 66–69.
[20] S. Grazulis, D. Chateigner, R.T. Downs, A.F. Yokochi, M. Quiros, L. Lutterotti, E. Manakova, J. Butkus, P. Moeck, A. Le Bail, Crystallography open database - an open-access collection of crystal structures, J. Appl. Crystallogr. 42 (Pt 4) (2009) 726–729.
[21] M. Gaeini, S.A. Shaik, C.C.M. Rindt, Characterization of potassium carbonate salt hydrate for thermochemical energy storage in buildings, Energy Build 196 (2019) 178–193.
[22] M. Reynaud, Design of new sulfate-based positive electrode materials for Li- and Na-ion batteries. University of picardie jules verne HAL archives, 2014.

[23] M. Weil, On the (non-)existence of Tutton salts with formula types [M(H2O)(6)](ClO4)(2)(H2O)(2) and Na2M(SO4)(2)(H2O)(6) (M is a first-row transition metal), Acta Crystallogr. C 69 (2013) 990–994.
[24] L.C. Sögütoglu, P.A.J. Donkers, H.R. Fischer, H.P. Huinink, O.C.G. Adan, In-depth investigation of thermochemical performance in a heat battery: cyclic analysis of K2CO3, MgCl2 and Na2S, Appl. Energy 215 (2018) 159–173.
[25] W.N. Wermink, G.F. Versteeg, The oxidation of Fe(II) in acidic sulfate solutions with air at elevated pressures. Part 1. Kinetics above 1 M H2SO4, Ind. Eng. Chem. Res. 56 (14) (2017) 3775–3788.